The Aeronautical Journal (2022), 1–18
doi:10.1017/aer.2022.51

REGULAR PAPER
2022 ISABE Conference Paper

On the effect of inter compressor duct length on compressor performance

T. Dygutsch*, A. Kasper and C. Voss

German Aerospace Center (DLR), Institute of Propulsion Technology, Cologne, Germany
*Corresponding author email: thomas.dygutsch@dlr.de

Received: 21 October 2021; **Revised:** 15 March 2022; **Accepted:** 20 April 2022

Keywords Axial compressor; Inter-compressor duct; Aerodynamics; Optimisation; low-pressure compressor; high-pressure compressor

Abstract

Compression systems of modern, civil aircraft engines consist of three components: Fan, low-pressure compressor (LPC) and high-pressure compressor (HPC). The efficiency of each component has improved over the last decades by means of rising computational power which made high level aerodynamic optimisations possible. Each component has been addressed individually and separated from the effects of upstream and downstream components. But as much time and effort has been spend to improve performance of rotating components, the stationary inter-compressor duct (ICD) has only received minor attention. With the rotating compression components being highly optimised and sophisticated their performance potential is limited. That is why more aggressive, respectively shorter, ICDs get more and more into the focus of research and engine manufacturers. The length reduction offers high weight saving and thus fuel saving potential as a shorter ICD means a reduction in aircraft engine length. This paper aims at evaluating the impact of more aggressive duct geometries on LPC and HPC performance. A multi objective 3D computational fluid dynamics (CFD) aerodynamic optimisation is performed on a preliminary design of a novel two spool compressor rig incorporating four different operating line and two near-stall (NST) conditions which ensure operability throughout the whole compressor operating range. While the ICD is free to change in length, shape and cross-section area, the blades of LPC and HPC are adjusted for changing duct aerodynamics via profile re-staggering to keep number of free parameters low. With this parametrisation length, reductions for the ICD of up to 40% are feasible while keeping the reduction in isentropic efficiency at aerodynamic design point for the compressor below 1%pt. Three geometries of the Pareto front are analysed in detail focusing on ICD secondary flow behaviour and changes of aerodynamics in LPC and HPC. In order to asses changes in stall margin, speedlines for the three geometries are analysed.

Nomenclature

Greek letters

Π_t	total pressure ratio
Θ	slope angle
ω_t	$= \frac{p_{t,in} - p_{t,out}}{p_{t,in} - p_{in}}$, total pressure loss coefficient

Latin letters

$\dot{m}_{corr}$	corrected mass flow rate
A	area
H	height
L	length
R	radius

This paper is a version of a presentation due to be given at the 2022 ISABE Conference

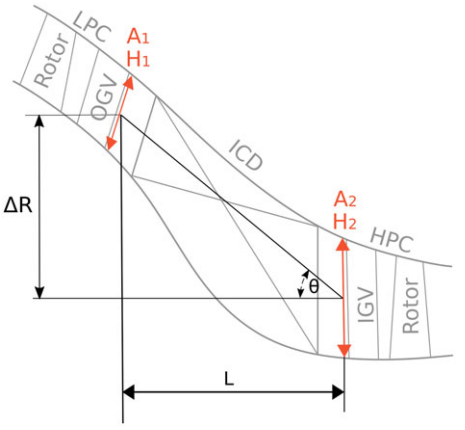

Figure 1. *Geometric ICD definitions.*

1.0 Introduction

The design process of gas turbines is a highly complex and interdisciplinary task. To make this complexity manageable the main components of the gas turbines are subdivided into modules. Jarrett et al. [1] state, that this holds the possibility to create engine families with different thrust classes and enable re-designs of single modules. But this modularity comes at a cost: Module interfaces are artificial design boundaries restricting the design space. In preliminary design Ghisu et al. [2, 3] showed that expanding the design space by removing artificial module boundaries holds potential for further efficiency improvements. Consequently the same must be true in detailed 3D design which until now is still carried out on a component (i.e. LPC) or even sub-component level (i.e. single stage) where design boundaries are set by radial distributions of flow quantities. In most studies the ICD has been analysed as a stand-alone component without considering the influence of neighbouring components.

The ICD flow field is very complex and strongly influenced by radial and axial pressure gradients, which are more pronounced as the duct is designed more aggressive, meaning shorter and stronger curved (compare Britchford et al. [4]).

The aggressiveness of the ICD geometry is defined in literature (compare Naylor et al. [5] and Wallin et al. [6]) by the change of R over the axial length L giving the slope $\Delta R/L$ or the slope angle Θ as can be seen in Fig. 1. The rate of diffusion done in the ICD is defined by the area ratio between in- and outlet A_2/A_1 and the non-dimensional length H_1/L. H_1 and H_2 correspond to the channel height at these locations. The definition of the inlet and outlet of the ICD is key when it comes to comparing different kinds of ICDs. In modern aero-engines the LPC rotor and outlet guide vane (OGV) already have a declining hub. This is in contrast to most rigs presented in literature. For this reason we follow the geometric definition of Wallin et al. [6]. It defines the ICD by the neighbouring OGV trailing and inlet guide vane (IGV) leading edge (see Fig. 1).

Ortiz Dueñas [7] have been studying the influence of duct length by analysing three different linear-cascade ducts without structural struts. It showed that secondary losses increase with shorter geometries leading to separation at hub and shroud endwall for the shortest one.

Naylor et al. [5] used the same duct geometries as Ortiz Dueñas et al. [7] and integrated a strut in one of the duct geometries that significantly increased the losses. It turned out that aggressive ducts are prone to hub-strut corner separations due to superposition of endwall and strut diffusion. To suppress this type of corner separation endwall contouring has been used.

In aero-engine applications struts do serve two purposes, which are defined by Britchford [8] and Naylor et al. [5] as follows: First, they are structural elements that carry loads from the engine core to the outer structure. Second, they are needed to feed services such as cooling air and oil and allow the radial drive shaft to traverse the duct.

https://doi.org/10.1017/aer.2022.51 Published online by Cambridge University Press

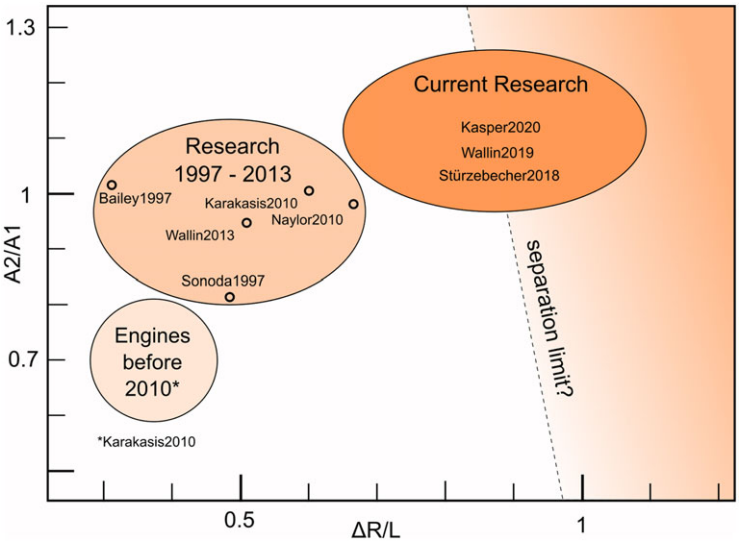

Figure 2. *Area ratio A2/A1 vs slope* $\Delta R/L$ *of ICD geometries from test compressors and aero-engines.*

A first estimation of the effects caused by an upstream stage/compressor on ICD performance has been carried out by Sonoda et al. [9, 10]. For this purpose varying inlet conditions have been applied at ICD inlet. The boundary layer thickness influences the size of horseshoe vortex and therefore the area of low total pressure entering the HPC. Influence of swirl on ICD flow behaviour has been studied by Ref. [11] and Gao et al. [12]. Reference [11] showed a reduction in pressure gradient at hub and shroud but a rise in losses for a non-struted ICD. Gao et al. [12] studied the same effect on a struted ICD. Results proved a significant dependency of secondary flow structure on swirl angle.

The influence of an upstream stage has been analysed by Bailey et al. [13]. The stage caused the total pressure losses to increase significantly. The authors could not determine whether these losses are wake mixing losses or losses directly linked to the ICD.

Karakasis et al. [14] also studied the impact of an upstream stage finding that the stage encounters a varying backpressure over the circumference. This variation is enforced by the upstream potential field of the strut, which leads to a variation of stage throttling over the circumference. The aforementioned test compressor rigs from literature have been classified in terms of area ratio and slope in Fig. 2. A hypothetical separation limit in terms of area ratio and slope is indicated. Lower area ratios lead to lower diffusion in the ICD, pushing separation limit and enabling higher slopes. As an orientation, aero-engine ICD designs from before 2010 are added from Karakasis et al. [14]. It can be found that engine applications in comparison with research use more conservative ICD designs. Naylor et al. [5] say that this is because the annulus line needs to be fixed early in aero-engine design, and designers don't want to take the risk of possible strut-hub corner separations.

Most of the experiments from literature are carried out on low-speed test facilities as lower speed means lower stresses and therefore lower hardware and testing costs as Ref. [15] points out. One of the first aero-engine like ICD high-speed tests in open literature has been run by Wallin et al. [16]. The high-speed regime has the advantage to operate the ICD under engine realistic flow conditions in terms of Reynolds and Mach number.

At DLR's test facility of the Institute of Propulsion Technology, a series of tests on next generation geared engine compression system is conducted. Therefore highly aggressive ICD configurations are evaluated under engine realistic flow conditions in a joint undertaking with MTU Aero Engines and GKN Aerospace within the European Clean Sky 2 research and innovation program.

The intention has been to set up three different ICD rigs in terms of aggressiveness and level of component interaction. The first two rigs are non-rotating full annulus ICD rigs with different $\Delta R/L$

https://doi.org/10.1017/aer.2022.51 Published online by Cambridge University Press

consisting of LPC OGV, strut and HPC IGV. The design intends the first one (A) to be fairly aggressive – compared to currently flying applications – with stable flow condition, and the second one (B) to be even more aggressive with flow separation occurring in the ICD. The rigs are highly instrumented by a vast number of static pressure probes and high accuracy traverse measurements. The rigs have been running at multiple operating points ranging from idle over design to maximum take-off operating conditions. The focus of these high effort measurements has been to further explore ICD design space and to confirm the ability of the DLR flow solver TRACE to reproduce measured flow quantities and phenomena (i.e. flow separation). A first comparison of traverse measurements versus CFD results at the strut exit plane in Fig. 4 shows satisfactory agreement between the acquired data and simulation results. An overview on the test campaign, considered operating points and CFD results of both rigs are given by Wallin et al. [6].

A numerical study by Stürzebecher et al. [17] on the potential of ICD length saving showed that length reductions of up to 30% are possible but leading to flow separation. As baseline ICD rig (A) has been used, of which the OGV and struts have been modelled as studies of Britchford et al. [18] and Karakasis et al. [14] show that the OGV wakes are having a high impact on aerodynamic stability of the ICD.

First results of the extensive high-speed testing of the ICD rig (A) and (B) have been presented by Kasper et al. [19]. Oil-streak paint showed for rig (B) severe flow separation in the ICD hub region. In an aerodynamic optimisation by Stürzebecher et al. [17] this separated ICD (B) has been stabilised with a hub endwall contouring supported by a locally bowed strut trailing edge that leads to suppression of hub-strut corner separation. To the authors knowledge this ICD is the most aggressive duct still separation free and therefore defines the current separation limit (compare Fig. 2).

So far duct designs have gotten more aggressive over time (compare Fig. 2) but interaction with upstream compressors have received very limited attention. To the authors knowledge no publication has yet assessed the influence of an aggressive ICD geometry on downstream compressor component.

This will be the purpose of the third and last rig in the aforementioned test campaign. It is supposed to reflect engine-like environment and interactions between the different compression components. The rig is set up as a two-spool test compressor consisting of LPC, ICD and HPC representative of next generation geared engine compression systems and will be tested by the end of 2022.

In the paper at hand a preliminary 3D design of the two-spool compressor rig is used to carry out a study on the performance influence of ICD length reduction on the LPC and HPC. The study is performed as an aerodynamic optimisation. While the ICD can vary in length and shape, the blades of LPC and HPC are re-staggered at profile level to account for changes in duct aerodynamics. To ensure operability throughout the whole compressor operating range, six operating conditions are considered. The results are first analysed on a global Pareto front level to estimate the impact of ICD length reduction on losses/efficiency at component level. Afterwards three designs of the Pareto front of different ICD lengths are analysed in terms of ICD secondary flow structure and radial flow distortions on LPC and HPC. In the end speedline calculations of the three designs are performed to estimate the impact on stall margin (SM).

2.0 Setup of optimisation study

The baseline compressor used for the conducted study is a preliminary 3D design of the novel two spool test compressor. It is representative for next generation modern civil aircraft applications and can therefore be considered as state of the art. For this study a subset of the rig has been used to reduce 3D CFD simulation time. The actual two-spool compressor rig consists of 1.5 stages LPC, ICD and a 4.5 stages HPC of which the four HPC stages – excluding the IGV – have been previously aerodynamically optimised with the method presented by Schnoes et al. [20].

For the study presented the setup is reduced to the last LPC stage, the ICD and 2.5 HPC stages. The two HPC stages are transonic. As a reference the ICD length is 12% shorter than the ICD duct (A)

https://doi.org/10.1017/aer.2022.51 Published online by Cambridge University Press

Table 1. *Operating conditions: Compressor spool speeds and bleed rates*

	LPC n/N (%)	HPC n/N (%)	Bleed rate (%)
Idle speed (IDL) @ OL	35	78	10
Part speed (PRT) @ OL, NST	75	92	3
Design speed (DSG) @ OL, NST	100	100	3
Over speed (OVR) @ OL	110	105	3

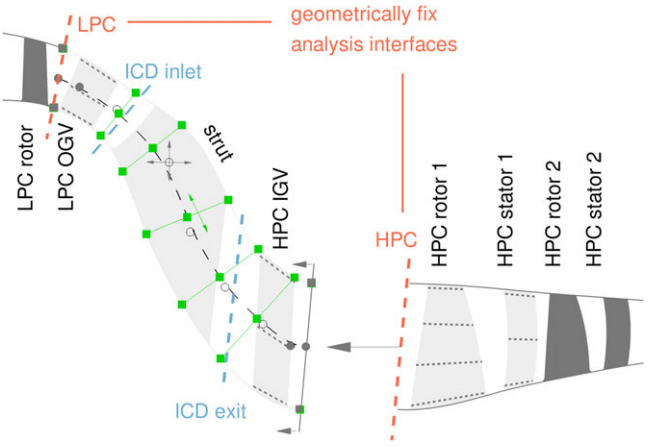

Figure 3. *Flowpath and blade parameterisation.*

mentioned before. A bleed slot is located between the LPC and the ICD to ensure operability. The bleed rate and operating points considered for the current analysis are presented in Table 1. The IGV and both HPC stators are variable vanes, which are adjusted for each operating condition during the study.

2.1 Optimisation method

For the current study the optimisation suite AutoOpti has been used. It has been developed by DLR at the Institute of Propulsion Technology for the purpose of turbomachinery application. An evolutionary algorithm is the foundation for the underlying optimisation process that creates new candidates by mutation and differential evolution. A process chain is executed and evaluated for each candidate whereby the values of objective functions and constraints are retained. To improve the process of candidate selection metamodels are used. For further explanations regarding the optimisation process and the use of metamodels the encouraged reader is referred to Voss et al. [21] and Siller et al. [22].

2.2 Design parameters

The flowpath and blades are parameterised (marked in light grey in Fig. 3) in a way that the ICD can vary in axial length.

The flowpath is parameterised between the interface of LPC rotor/OGV and HPC IGV/rotor 1 as can be seen in Fig. 3 marked by filled squares. It is based on a b-spline curve (marked as dashed line) which is defined by nine control points (marked by circles) and acts as a spine for the flowpath. Four of the control points are fixed (filled circles) – two at the front, two at the rear – which ensures a fixed inclination to the LPC and the HPC. The remaining five control points (non-filled circles) are free to move in axial and radial direction (ten parameters). On the spine five points (green squares) are free to

https://doi.org/10.1017/aer.2022.51 Published online by Cambridge University Press

move along the spine (five parameters). At these positions a height is applied rectangular to the spine (five parameters) which then defines the hub and shroud contour. All these points are defined relative to the corner points (dark grey squares) as the right corner points are free to move in axial direction giving the possibility to shorten the ICD. Both right corner points are controlled by one parameter, meaning they are shifted in axial direction by the same amount.

With a reduction in ICD length the strut needs to be reduced in chord length to fit the shorter duct geometry. As the strut leading edge position is fixed, the trailing edge needs to be moved in order to vary the strut in length. Therefore it is parametrised by the two points at which the strut trailing edge intersects with the flowpath. As stated in the introduction struts fulfil two purposes: First, as a structural element and second, to feed services like air and oil. In the present study no structural calculations are performed as information about forces transmitted through the struts is proprietary. To at least maintain the ability to carry services the maximum thickness of the strut is kept constant with a reduction in chord length.

As the ICD is reduced by a delta in axial length the IGV is moved by the same delta in axial direction to the front. The strut trailing edge is defined by keeping the same approximated distance $\sqrt{\delta x^2 + \delta r^2}$ at hub and shroud between IGV leading and strut trailing edge intersections. This approach leads to a slightly varying axial distance between strut and IGV, but maintains approximately the distance the flow has to cover between the two vanes. The blades in light grey – except the strut – are parametrised on three profiles for the stators and four profiles for the rotor (indicated by dotted lines) allowing the profile stagger angle to be varied. The blades in dark grey are unchanged in the optimisation process. The whole configuration is therefore parametrised by 34 free parameters.

2.3 Steady-state RANS setup

The 3D CFD Reynolds-averaged-Navier-Stokes (RANS) steady state, fully turbulent calculations are performed with DLR's TRACE Suite. TRACE has been developed explicitly for turbomachinery purposes and has been calibrated and validated in many turbo machinery projects [23–25].

A setup study has been performed previously by Stürzebecher et al. [17] to determine which turbulence model and rotational fix is best suited for the simulation of ICDs. As the calibrated and validated combination of k-ω turbulence model with Kato-Launder stagnation point fix and Bardina rotational effects extension (for further details compare Röber et al. [26]) is applied to blade rows located in the more axial parts of the flow path, ICD flow is modelled using the streamline curvature (SLC) rotational effects extension. As rotation of flow in the ICD not only occurs about the circumference but also in axial direction the modelling of this effect plays a major role for ICD flow simulation. Furthermore the mentioned study [17] determined the influence of multi blade vs single blade passage(s) on flow structure in the ICD. CFD results with the aforementioned settings are compared with first measurement results for the ICD rig (A) in Fig. 4. Total pressure quantities are evaluated for a full strut passage and CFD results are interpolated onto the measurement grid. CFD results are in agreement with measurements. The level of total pressure in the experiment is slightly higher.

The fully structured mesh is generated using NUMECA Autogrid. To ensure low mesh uncertainty and low computational time, a mesh study has been performed on the actual two-spool compressor rig setup. The mesh settings for the smaller optimisation setup are derived from the full rig. Four different meshes are compared to each other in terms of isentropic efficiency and number of cells used in Fig. 5. Mesh M3 shows the best compromise as the sensitivity is lower compared to M2 and uses only half the number of cells as M4.

The setup in the present paper is carried out as single blade passage calculation with mixing planes on a structured multi-block grid with 6.3 million cells. Between 61 and 89 cells in spanwise direction with 19 cells in rotor gaps and 13 in variable stator half gaps. A bleed port is simulated by a bleed boundary condition between OGV and strut. The dimensionless wall coordinate y^+ is for the majority of the endwalls/blades between 0.8 and 1.2. All rotors have fillets at the hub. The OGV and strut have fillets at both hub and shroud. The IGV and the first two stators of the HPC are adjustable and therefore

https://doi.org/10.1017/aer.2022.51 Published online by Cambridge University Press

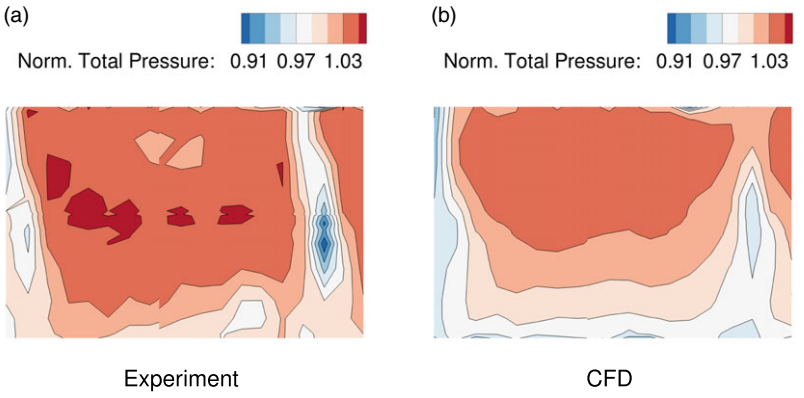

Figure 4. *Comparison of ICD rig (a) measurements vs CFD simulation at ICD exit plane at design point.*

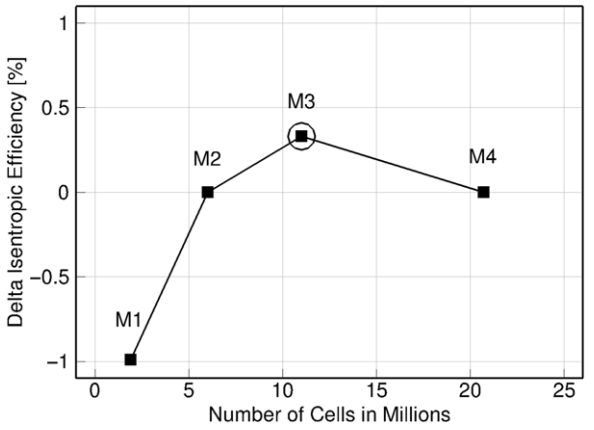

Figure 5. *Meshstudy for the actual two-spool compressor rig.*

have half gaps at hub and shroud. Convergence is reached when the compressor, all stages and all rows reach mass flow variation of 0.05% and efficiency variation of 0.2% over 1,000 time steps.

2.4 Objectives and constraints

For each compressor geometry four different operating line conditions are simulated (Table 1), which represent the following operating conditions idle speed (IDL), part speed (PRT), design speed (DSG) and over speed (OVR). For PRT and DSG corresponding near stall operating points are calculated as indicated in Fig. 6. A newly created compressor geometry is only considered successful if it passes the complete process chain which implies convergence of all six operating points. Mass flow rate is allowed to vary by $\pm 1\%$ for all operating line conditions. The allowed mass flow range is indicated by light grey margins in Fig. 6. For near stall operating points the mass flow rate is allowed to fall below the initial value, but the pressure ratio needs at least to maintain the initial value – meaning the stall margin needs to be kept or increased. The allowed mass flow rate and total pressure ratio for near stall operating points are indicated by the dark grey areas in Fig. 6. All operating points are simulated with a backpressure boundary condition. Further constraints are set to keep limits for the area of low wall shear stresses of OGV and strut, as has been applied in previous studies (comp. Stürzebecher et al. [17]). All cell faces with a wall shear stress below five are summed up resulting in a wetted area with very low wall shear

https://doi.org/10.1017/aer.2022.51 Published online by Cambridge University Press

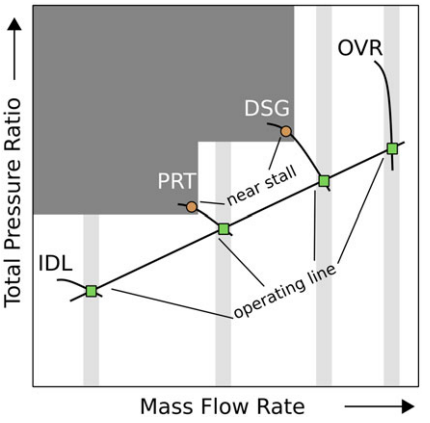

Figure 6. *Compressor map with operating points and constraints in mass flow rate and total pressure ratio: Light grey – operating line constraints, dark grey – near stall constraints.*

stresses. This type of constraint has been proven very useful in reducing flow separation tendency in the ICD. These constraints are applied to all operating points.

The two objective functions of the optimisation are to minimise ICD length and maximise isentropic efficiency for the compression system at DSG operating line condition.

Each CFD simulation is carried out on 4x AMD EPYC 7601 (32 cores, 2.2GHz) central processing units with 256GB RAM. A fully passed process chain therefore takes approximately 1.5–2 hours to complete.

3.0 Results

In this section the results of the optimisation study are shown. At first a view at global optimisation results in form of Pareto front evaluation is undertaken to get an overview on how losses/efficiency evolve with reduction in ICD length. Afterwards three Pareto-optimal geometries are analysed in further detail to get deeper insights on ICD and LPC/HPC aerodynamic behaviour.

During the optimisation run time 3,869 geometries have been processed of which 2012 are successful and have passed the complete process chain. Almost all unsuccessful geometries failed due to non-convergence in the CFD simulations of one of the six operating points. Most of the time IDL or OVR operating line conditions failed.

3.1 Pareto analysis

In Fig. 7(a)–(c) the delta in isentropic efficiency for different components at all operating line conditions (see Table 1) is plotted over length reduction. Here, the reference is the isentropic efficiency for the geometry D0 with a length reduction of 0% at the corresponding operating line conditions (see Table 2). The Pareto front in regards to the optimisation objectives at DSG operating line condition is plotted in black in Fig. 7(a). The geometries that do not belong to Pareto front are blanked in all plots for clarity reasons. For better interpretation the data points are fitted via polynomial regression of second order.

For the compression system in Fig. 7(a) it can be noticed that the initial design can be improved by 1.2%pts. compared to geometries of the Pareto front at DSG operating line condition. For this operating point the efficiency drops by only 1%pt. for the shortest geometry which is surprising due to the very aggressive reduction in compressor length. The profile re-staggering seems to be sufficient to account

https://doi.org/10.1017/aer.2022.51 Published online by Cambridge University Press

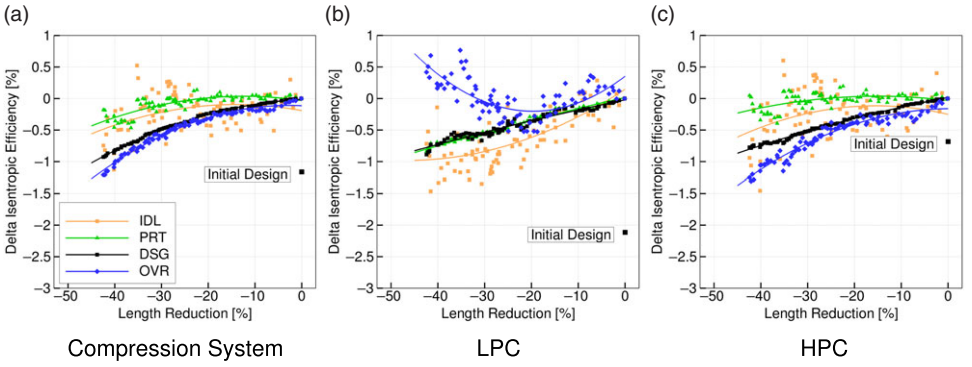

Figure 7. *Isentropic efficiency over ICD length reduction at operating line conditions.*

Table 2. *Non-dimensional geometric parameters of Pareto designs*

Geometry	Ax. Length Red.	Strut Chord Length Red. at hub/shroud	ΔR/L	A_2/A_1	H_1/L
D0	0%	2%/10%	0.93	1.23	0.19
D20	19%	13%/28%	1.08	1.58	0.23
D40	38%	24%/43%	1.40	1.52	0.31

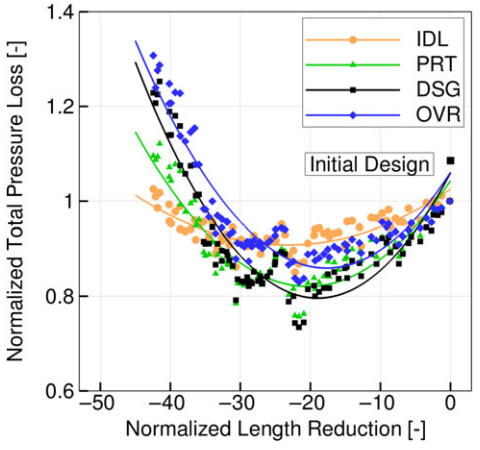

Figure 8. *ICD total pressure losses over length reduction.*

for changes in duct aerodynamics. All off-design operating conditions do also show declining efficiency in the same magnitude as for DSG operating line condition. The small increase in losses at off design can not be attributed to objective functions, but is a result of assured convergence (all geometries which do not converge in one operating point are marked as failed) and constrained operating point conditions.

As the global optimisation goal is to enhance efficiency at compression system level, the optimisation algorithm is free to make a trade-off between LPC and HPC efficiency. The resulting distributions of isentropic efficiency can be found in Fig. 7(b) and (c). Furthermore, it can be seen that the LPC efficiency is improved by 2%pts. and HPC efficiency by 0.7%pts. compared to initial design. Until now LPC and HPC component have been analysed in terms of efficiency. To evaluate the losses caused by the shortened duct itself the total pressure loss of the ICD ω_t is plotted in Fig. 8.

https://doi.org/10.1017/aer.2022.51 Published online by Cambridge University Press

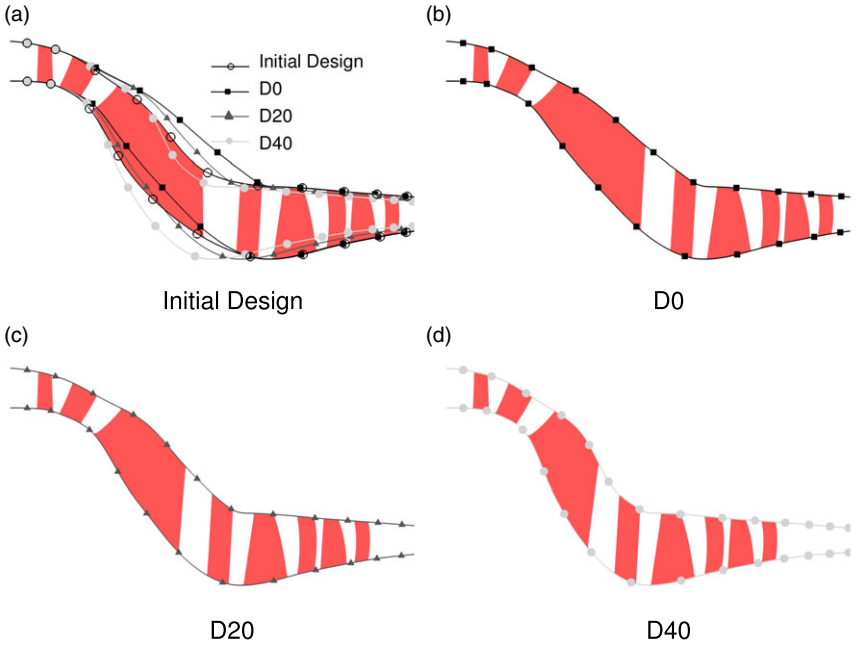

Figure 9. *Comparison of flowpath and blade geometries of D0, D20, D40 versus Initial Design.*

For modest length reductions a decrease in losses in all operating points can be noticed which has a minimum at approx. -20% length reduction. Shorter ducts again show a strong rise in losses. For the DSG operating line condition this effect is most pronounced and will be covered in more detail in the following. Initial ICD design has slightly higher losses as comparable Pareto designs.

3.2 Pareto designs

For a more detailed evaluation the geometries in Table 2 which represent the two extremes of 0% (D0) and close to 40% (D40) as well as one geometry with ca. 20% (D20) length reduction have been analysed at DSG operating line condition in the following. A comparison of the flowpaths of D0, D20 and D40 is shown in Fig. 9.

3.3 ICD secondary flows

The secondary flow structure in the ICD has a great impact on loss production and accordingly on the inlet conditions to the HPC. Hence streaklines and iso-surfaces of axial velocity equal to zero are used in the following to visualise flow structure and separation areas. Loss calculation is based on ICD inlet and exit planes indicated in Fig. 3.

Radial distribution of total pressure loss at ICDexit in Fig. 10 shows a loss increase with decreasing ICD length at the lower 30% relative height. Between 30 and 80% relative height the geometries D20 and D40 show a comparable distribution of losses which is lower then geometry D0. Between 80 and 85% relative height the losses for the shorter geometries D20 and D40 are slightly higher compared to D0.

The loss increase in the lower 30% can be traced back to a rise in secondary flow structures as can be seen in Figs 11(a)–(c). The non-axisymmetric flow field is a result of the not purely axial outflow of the OGV. The area of low total pressure close to strut trailing edge for D0 gets wider for the shorter geometry D20. For the shortest design D40 two independent areas of low total pressure have been formed to the

https://doi.org/10.1017/aer.2022.51 Published online by Cambridge University Press

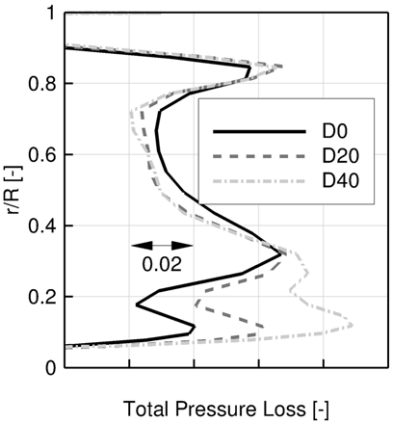

Figure 10. *ICD total pressure loss distribution at ICD exit at DSG operating line condition.*

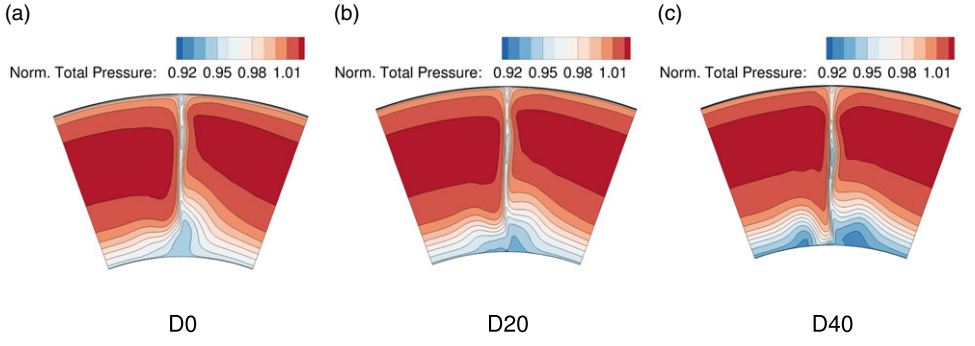

Figure 11. *Total pressure contours in S3 plane at ICD exit at DSG operating line condition; view against streamwise direction.*

left and right of the strut trailing edge. Furthermore for D40 the fluid with low total pressure is now covering the whole passage width.

In reference to Fig. 8 this means, that when ICD geometries get shorter the lower wetted area of strut and endwalls leads to lower losses. This is true until secondary losses rise faster then wetted area is decreased. Leading at first to a reduction and after a certain point to a rise in ICD losses.

The streaklines for D0, D20 and D40 over the strut surface in Fig. 12 do not show significant rise in secondary flows with decreasing ICD length. It can be seen that some fluid is entering the strut from the hub endwall but no hub-strut-corner separation can be detected. The secondary flow structure is most visible for design D0. Which means the shorter the duct gets the further away from the strut the secondary flow structure evolves, which underpins the findings of Fig. 11.

The streaklines for D0, D20 and D40 over the hub endwall in Fig. 13 show that geometry D0 is free of separation. For the shorter D20 and D40 small separation areas occur close to strut trailing edge. This is according to the low total pressure areas found in Fig. 11. The shorter the duct, the more pronounced the streaklines are showing a tendency to migrate in circumferential direction.

3.4 Radial influence on LPC/HPC

Until now the changes in duct aerodynamics and corresponding secondary flows have been assessed. To widen the view and get a better understanding on the influence of ICD length reduction on the LPC and

https://doi.org/10.1017/aer.2022.51 Published online by Cambridge University Press

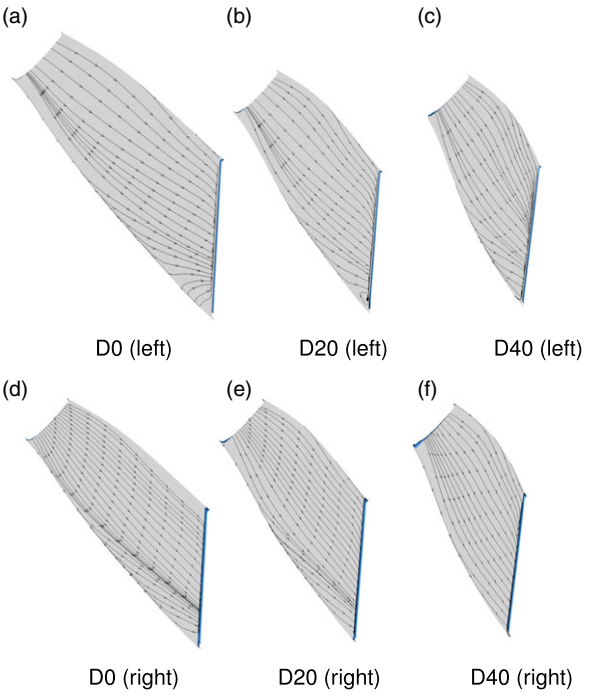

Figure 12. *Streaklines and iso-surfaces of axial velocity equal to zero at strut surfaces at DSG operating line condition. Left: in streamwise direction left. Right: in streamwise direction right.*

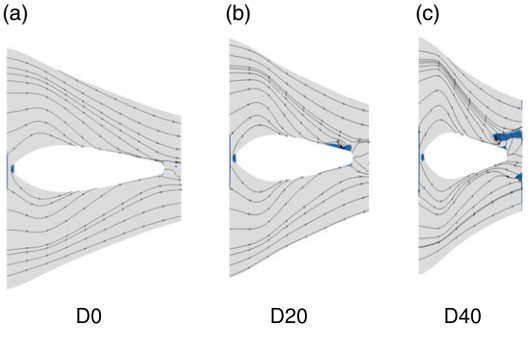

Figure 13. *Streaklines and iso-surfaces of axial velocity equal to zero at ICD hub endwall at DSG operating line condition.*

HPC components a closer look at the corresponding interfaces is indispensable. Due to the fact, that these interfaces underlie geometrical changes throughout the geometries D0, D20 and D40, specifically defined, geometrically fixed analysis interfaces are used which are indicated in Fig. 3. At the LPC analysis interface in Fig. 14 the changes in upstream effect of the ICD can be seen. It can be noticed that the flow between 0 and 50% relative height is accelerating from D0 to D40. At the same time the static pressure drops and the swirl angle decreases. The opposite behaviour can be found from 50 to 100% relative height. This phenomena is driven by the increasing curvature at the hub OGV trailing edge where the duct gets more aggressive (compare Fig. 9). This triggers a shift in mass flow from shroud to hub, leads to a radial shift in loading of the LPC rotor and results in a shift of total pressure from hub to shroud. As the distance between strut leading edge and OGV trailing edge is fixed the changes due to the upstream effect of the strut can be neglected.

https://doi.org/10.1017/aer.2022.51 Published online by Cambridge University Press

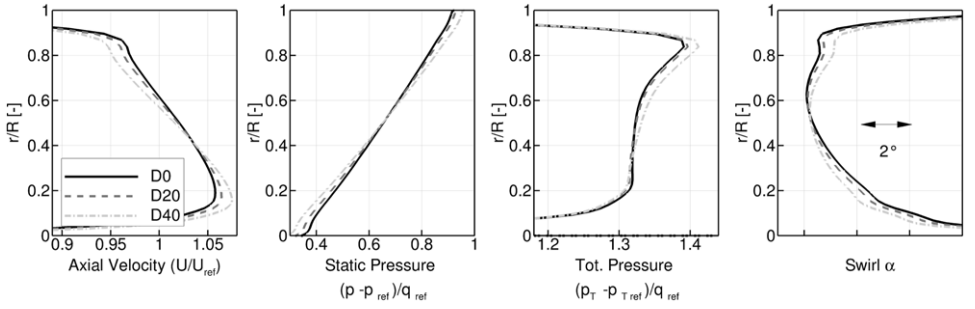

Figure 14. *Radial distributions at the LPC analysis interface (rotor/OGV) at DSG operating line condition.*

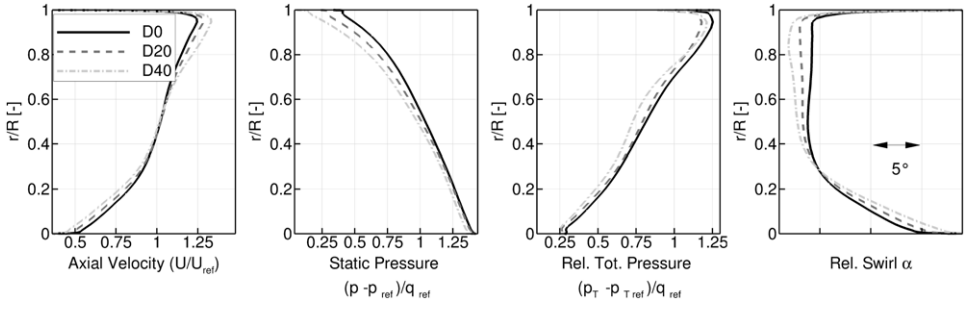

Figure 15. *Radial distributions at the HPC analysis interface (IGV/rotor 1) at DSG operating line condition.*

The downstream effect of changes in ICD aerodynamics can be seen in Fig. 15. It can be noted, that the axial velocity undergoes a shift from hub to shroud. The changes are therefore vice versa in comparison to the LPC interface. This behaviour again implies a redistribution in mass flow now from hub to shroud. The static pressure is dropping for the shorter duct geometries, most notable at the shroud. Total pressure shows a successive drop over the full channel height. The relative swirl changes are in line with changes in axial velocity: At the hub the rotor 1 sees a higher positive incidence whereas at the shroud the incidence becomes negative.

The influence of changed duct aerodynamics on LPC and HPC rotor loading can be seen in Fig. 16. The diffusion of the geometrically unchanged LPC rotor is rising at the shroud and declining at the hub. This fits well with the aforementioned shift in mass flow from shroud to hub. For the HPC rotor 1 an increase in diffusion for D20 and D40 is visible. The changes for rotor 1 are rather small as the geometry is free to adapt to the changes in flow conditions. In contrast the second HPC rotor is geometrically fixed and shows a rise in diffusion over the full span width for the D20 design. For the shorter D40 geometry a higher diffusion is observed at the lower 10 to 40% relative height. In this scenario rotor 1 is no longer able to maintain the demanded pressure ratio (compare Fig. A.1). To fulfill the overall pressure ratio demand rotor 2 compensates the loss by a higher loading.

3.5 Speedlines

In order to evaluate off-design performance and the influence on stall margin speedline calculations on the full compression system have been performed and analysed on component level for LPC, ICD and HPC. For stall margin definition it is referred to the one used by Ref. [27] in Equation (1).

$$\mathrm{SM} = 1 - \frac{\Pi_{\mathrm{t,\,OL}}}{\Pi_{\mathrm{t,\,Stall}}} \cdot \frac{\dot{m}_{\mathrm{corr,\,Stall}}}{\dot{m}_{\mathrm{corr,\,OL}}} \tag{1}$$

https://doi.org/10.1017/aer.2022.51 Published online by Cambridge University Press

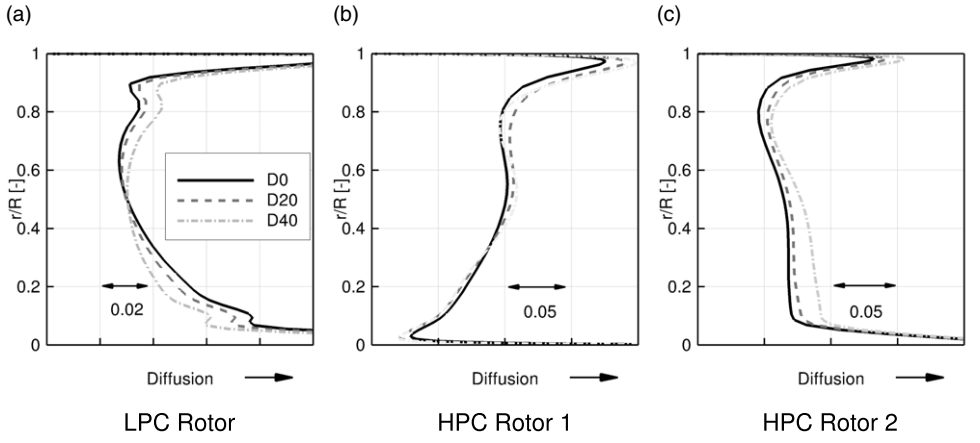

Figure 16. *Radial distribution of diffusion of LPC and HPC rotors at DSG operating line condition.*

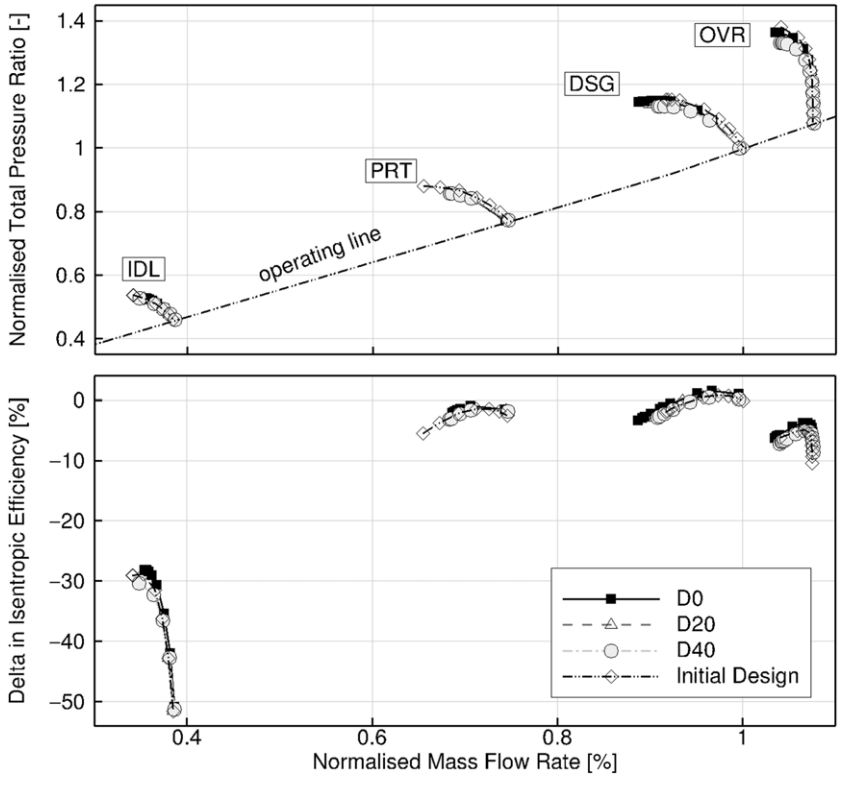

Figure 17. *Full compression system total pressure and isentropic efficiency speedlines.*

All four speedlines for the compression system are shown in Fig. 17. All values are normalised to the DSG operating line condition. Plotted are the three geometries D0, D 20, D40 and the initial design. It can be seen that initial design performance is matched very well by D0. IDL and OVR speedlines do show only a small reduction in SM which is a very satisfactory result as for these speeds only operating line conditions have been simulated. Keeping the SM at these speeds is linked to considering near stall operating points for PRT and DSG. PRT speedline shows a reduced SM but DSG therefore shows an

https://doi.org/10.1017/aer.2022.51 Published online by Cambridge University Press

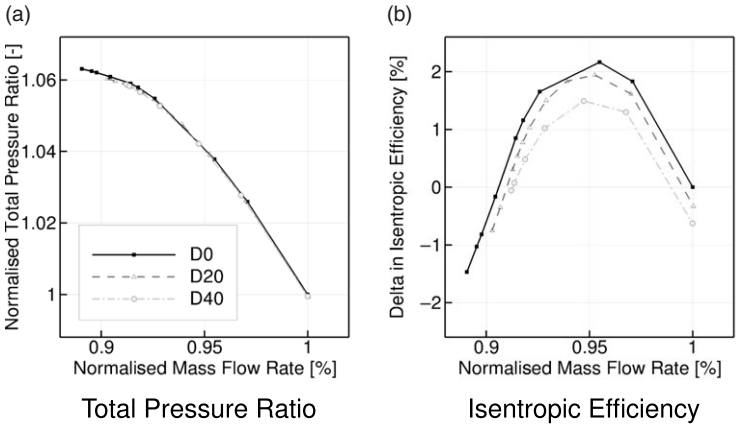

Figure 18. *LPC: DSG speedline.*

increase in SM for the optimised geometry. This trade-off is possible due to the fact that only near stall operating points for these speeds are considered and not the very last operating point before stall. The higher SM for DSG speed seems to be a result of the objective function which improves DSG operating line condition and therefore also influences stall behaviour. In the following only the optimised geometries will be discussed in more detail.

Comparing D0, D20 and D40 it can be noted that the overall impact of ICD length reduction on the compression system in terms of SM is rather low. Differences for IDL and PRT speedlines in SM are negligible. Larger differences can be observed for DSG and OVR speedlines. The SM for geometry D0 is 22% at the DSG speedline and is impacted the most by an ICD shortening. The D20 and D40 geometries show a drop in stall margin to 21 and 20% respectively. The relatively low reduction in SM can be attributed to the consideration of the near stall operating point in the optimisation process. As this speedline shows the most severe impact by duct length reduction, the corresponding component speedlines will be discussed in the ongoing. The DSG LPC speedlines are presented in Fig. 18. As has been discussed earlier the shorter ICD has some effect on the radial distribution of LPC rotor loading (compare Fig. 14). But neither the operating line (OL) condition or the speedline characteristic (slope) is influenced by that. Keeping in mind that full throttling to stall is not feasible in this setup since the HPC defines the stability limit. This means the last HPC stage stalls before even LPC can reach his specific stall limit.

The DSG HPC speedlines are plotted in Fig. 19. The difference in SM is visible in total pressure ratio Π_t and mass flow rate $\dot{m}_{\text{corr}}$ and is decreasing for shorter duct geometries. Geometry D0 has a SM of 22%. For designs D20 and D40 the SM is 21 and 19% respectively.

For the ICD the total pressure loss polar is plotted for the DSG speedline in Fig. 20. It can be found that losses are rising strongly when throttling the compression system. The losses for D0 and D20 are rising by 1.63 and 1.55 times but for D40 only by 1.2 times from operating line to stall.

4.0 Conclusion

An aerodynamic optimisation study on the performance influence of ICD length reduction on LPC and HPC has been conducted. As test vehicle a two-spool test compressor with 1 LPC stage, an aggressive ICD and 2.5 HPC stages is used. Four different operating points at the operating line and two at the near stall operating conditions are considered to assess the whole operating range of the compressor map and ensure full operability of the same. While the ICD is varied in length, shape and cross-section

https://doi.org/10.1017/aer.2022.51 Published online by Cambridge University Press

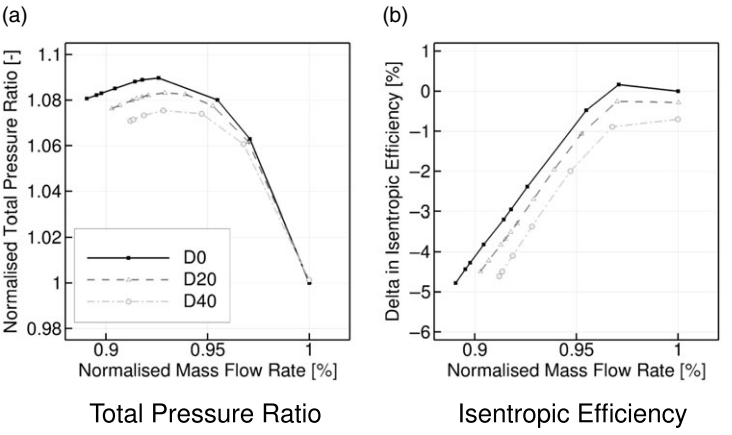

Figure 19. *HPC: DSG speedline.*

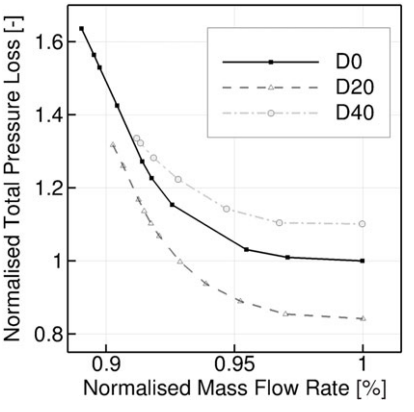

Figure 20. *ICD: DSG speedline in form of total pressure loss polar.*

are, the OGV, IGV and first HPC stage blades are adjusted for changing duct aerodynamics via profile re-staggering to keep number of free parameters low.

The optimisation results are evaluated globally on Pareto front level and later on three distinct Pareto designs with length reductions of 0% (D0), 19% (D20) and 38% (D40) are analysed in more detail. D20 and D40 do show minor separations at the hub endwall. No occurrence of hub-strut corner separation can be detected, which is surprising due to the highly aggressive duct geometries. The influence of stronger curvature and rising secondary flow losses on LPC and HPC performance has been studied by comparing LPC outlet and HPC inlet conditions and performing speedline calculations. The results showed for shorter ducts a radial shift of mass flow rate at both interfaces, which compressor blading needs to account for. Furthermore the increasing ICD secondary flow losses in the hub region need to be compensated by the HPC. To assess influence on stall margin speedline calculations are carried out. Results can be summarised as follows:

- First, a significant improvement from initial design to Pareto designs in efficiency and stall margin at design operating condition has been possible.
- Second, a very aggressive variation of ICD length reduction of up to 40% has been evaluated showing that the decrease in isentropic efficiency and stall margin can be limited to respectively 1%pt. and 2%pts. at design condition.

https://doi.org/10.1017/aer.2022.51 Published online by Cambridge University Press

The fairly low impact on compressor efficiency and stall margin and the absence of hub-strut corner separations in the ICD can be attributed to the well suited optimisation and parametrisation strategy.

Acknowledgement. This project has received funding from the Clean Sky 2 Joint Undertaking (JU) under the European Union's Horizon 2020 research and innovation program under grant agreement no. 945541.

References

[1] Jarrett, J.P., Ghisu, T. and Parks, G.T. On the coupling of designer experience and modularity in the aerothermal design of turbomachinery, *J. Turbomach.*, 2009, **131**, (3), p 031018.

[2] Ghisu, T., Parks, G.T., Jarrett, J.P. and Clarkson, P.J. An integrated system for the aerodynamic design of compression systems—part I: Development, *J. Turbomach.*, 2011, **133**, (1), p 011011.

[3] Ghisu, T., Parks, G.T., Jarrett, J.P. and Clarkson, P.J. An integrated system for the aerodynamic design of compression systems—part II: Application, *J. Turbomach.*, 2011, **133**, (1), p 011012.

[4] Britchford, K.M., Carrotte, J.F., Stevens, S.J. and McGuirk, J.J. The development of the mean flow and turbulence structure in an annular S-shaped duct, *Volume* **1:** *Turbomachinery. ASME 1994 International Gas Turbine and Aeroengine Congress and Exposition*, American Society of Mechanical Engineers, The Hague, Netherlands, 1994, V001T01A144.

[5] Naylor, E.M.J., Dueñas, C.O., Miller, R.J. and Hodson, H.P. Optimisation of nonaxisymmetric endwalls in compressor S-shaped ducts, *J. Turbomach.*, 2010, **132**, (1), p 011011.

[6] Wallin, F., Langholf, P. and Nicke E. Aerodynamic test campaign of next generation aggressive intermediate compressor ducts, ISABE, Canberra, Australia, 2019, p 10.

[7] Ortiz Dueñas, C., Miller, R.J., Hodson, H.P. and Longley, J.P. Effect of length on compressor inter-stage duct performance, *Volume* 6: *Turbo Expo* 2007, *Parts A and B*. ASME Turbo Expo 2007: Power for Land, Sea, and Air. Montreal, Canada: ASME, 2007, pp 319–329.

[8] Britchford, K.M. *The Aerodynamic Behaviour of an Annular S-shaped Duct*, Thesis, Loughborough University, 1998.

[9] Sonoda, T., Arima, T. and Oana, M. The influence of downstream passage on the flow within an annular S-shaped duct, *Volume* **1:** *Turbomachinery. ASME 1997 International Gas Turbine and Aeroengine Congress and Exhibition*. Orlando, Florida, USA, 1997, p 14.

[10] Sonoda, T., Arima, T. and Oana, M. The effect of inlet boundary layer thickness on the flow within an annular S-shaped duct, *Volume* **1:** *Turbomachinery. ASME 1998 International Gas Turbine and Aeroengine Congress and Exhibition*. Stockholm, Sweden, 1998, p 11.

[11] Bailey, D.W. and Carrotte, J.F. The influence of inlet swirl on the Flow within an annular S-shaped duct, *Volume* **1:** *Turbomachinery. ASME 1996 International Gas Turbine and Aeroengine Congress and Exhibition*, ASME, Birmingham, UK, 1996, V001T01A016.

[12] Gao, L., Deng, X., Feng, X. and Yang, Z. Effect of inlet conditions on compressor intermediate duct, Proc. Inst. Mech. Eng. Part G J. Aerospace Eng., 2015, **229**, (6), pp 1154–1168.

[13] Bailey, D.W., Britchford, K.M., Carrote, J.F. and Stevens, S.J. Performance assessment of an annular S-shaped duct, J. Turbomach., 1997, **119**, (1), p 149.

[14] Karakasis, M.K., Naylor, E.M.J., Miller, R.J. and Hodson, H.P. The effect of an upstream compressor on a non-axisymmetric S-duct, *Volume* 7: *Turbomachinery, Parts A, B, and C*. ASME Turbo Expo 2010: Power for Land, Sea, and Air, ASME, Glasgow, UK, 2010, pp 477–486.

[15] Wisler, D.C. Loss reduction in axial-flow compressors through low-speed model testing, *J. Eng. Gas Turbines Power*, **107**, (2), 1985, pp 354–363.

[16] Wallin, F., Olsson, J., Johansson, P.P.J., Krüger, E. and Olausson, M. High speed testing and numerical validation of an aggressive intermediate compressor duct, *Volume 6B: Turbomachinery*. ASME Turbo Expo 2013: Turbine Technical Conference and Exposition, ASME, San Antonio, Texas, USA, 2013, V06BT38A003.

https://doi.org/10.1017/aer.2022.51 Published online by Cambridge University Press

[17] Stürzebecher, T., Goinis, G., Voss, C., Sahota, H., Groth, P. and Hammer, S. Automated aerodynamic optimisation of an aggressive S-shaped intermediate compressor duct, *Volume 2D: Turbomachinery*. ASME Turbo Expo 2018: Turbomachinery Technical Conference and Exposition, American Society of Mechanical Engineers, Oslo, Norway, 2018, V02DT46A002.
[18] Britchford, K., Manners, A., McGuirk, J. and Stevens, S. Measurement and prediction of flow in annular S-shaped ducts, *Exp. Thermal Fluid Sci.*, 1994, **9**, (2), pp 197–205.
[19] Kasper, A., Hergt, A., Stürzebecher, T., Grund, S., Flamm, J. and Nicke, E. Flow structure within an aggressive S-shaped intermediate compressor duct, *J. Phys. Conf. Ser.*, 2021, **1909**, (1), p 012025.
[20] Schnoes, M., Voÿ, C. and Nicke, E. Design optimisation of a multi-stage axial compressor using throughflow and a database of optimal airfoils, J. Global Power Propul. Soc., 2, 2018, W5N91I.
[21] Voss, C., Aulich, A. and Raitor, T. Metamodel assisted aeromechanical optimisation of a transonic centrifugal compressor, 15th International Symposium on Transport Phenomena and Dynamics of Rotating Machinery, ISROMAC-15, ISROMAC-15. 2015, p 8.
[22] Siller, U., Voÿ, C. and Nicke, E. Automated multidisciplinary optimisation of a transonic axial compressor, 47th AIAA Aerospace Sciences Meeting Including The New Horizons Forum and Aerospace Exposition, American Institute of Aeronautics and Astronautics, Orlando, Florida, 2009.
[23] Elfert, M., Weber, A., Wittrock, D., Peters, A., Voss, C. and Nicke, E. Experimental and numerical verification of an optimisation of a fast rotating high-performance radial compressor impeller, *J. Turbomach.*, 2017, **139**, (10), p 101007.
[24] Reutter, O.K., Ashcroft, G., Nicke, E. and Kuegeler, E. Comparison of experiments, full-annulus-calculations and harmonic-balance-calculations of a multi-stage compressor, *J. Global Power Propul. Soc.*, 2018, p 9.
[25] Reutter, O., Ashcroft, G., Nicke, E. and Kuegeler, E. Unsteady full annulus multi-stage compressor calculations - details on CFD-experiment comparison, Aerospace Europe 6th CEAS Conference, 2017, p 9.
[26] Röber, T., Kožulović, D., Kügeler, E. and Nürnberger, D. Appropriate turbulence modelling for turbomachinery flows using a two-equation turbulence model, in: *New Results in Numerical and Experimental Fluid Mechanics V*. Ed. by Rath, H.-J. et al. Red. by Hirschel, E.H. et al., vol. 92, Notes on Numerical Fluid Mechanics and Multidisciplinary Design (NNFM), Springer, 2006, Berlin, Heidelberg, pp 446–454.
[27] Cumpsty, N.A. *Compressor Aerodynamics*, Longman Scientific & Technical; John Wiley, 1989, Harlow, Essex, UK; New York.

A. Appendix

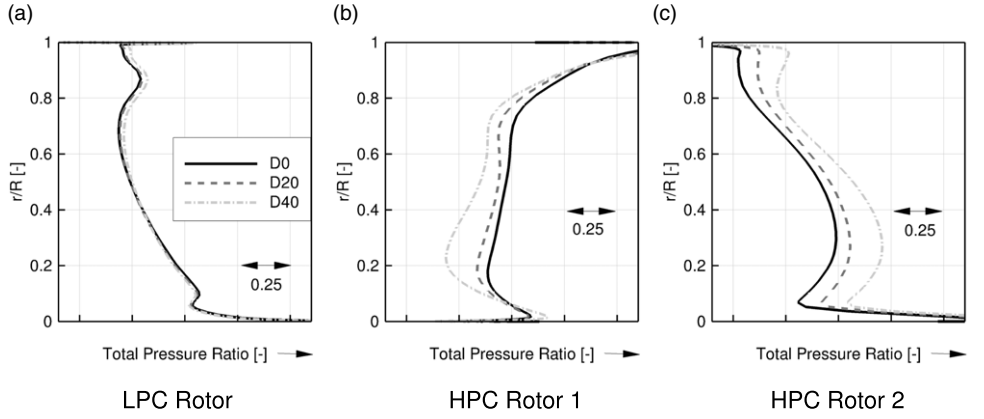

Figure A.1. *Radial distribution of total pressure ratio of LPC and HPC rotors at DSG operating line condition.*

Cite this article: Dygutsch T., Kasper A. and Voss C. On the effect of inter compressor duct length on compressor performance. *The Aeronautical Journal*, https://doi.org/10.1017/aer.2022.51